

CrossMark
click for updatesCite this: *RSC Adv.*, 2017, 7, 4791

Al doping effects on LiCrTiO₄ as an anode for lithium-ion batteries

Xiang Li, Yangyang Huang, Yuyu Li, Shixiong Sun, Yi Liu, Jiahuan Luo, Jiantao Han and Yunhui Huang

Al-Doped LiCrTiO₄ anode materials are successfully synthesized by a conventional solid-state reaction. Their structural and electrochemical properties are systematically investigated. With increasing the Al doping level (*x*), the lattice parameters of LiAl_{*x*}Cr_{1-*x*}TiO₄ get smaller. Meanwhile, asymmetric polarization was significantly reduced during the charge/discharge process, in contrast to an enhanced compatibility of electrode materials with organic electrolyte. The Al-doped LiAl_{0.2}Cr_{0.8}TiO₄ anode can still keep a discharge capacity of 123 mA h g⁻¹ at 1C for 100 cycles and 109 mA h g⁻¹ at 2C. More importantly, the Al-doped LiAl_{0.2}Cr_{0.8}TiO₄ anode exhibits remarkable electrochemical properties at a high-temperature of 60 °C with a very stable capacity of about 145 mA h g⁻¹ at 1C, and is promising as a high-performance anode.

Received 21st October 2016
Accepted 1st December 2016

DOI: 10.1039/c6ra25599j

www.rsc.org/advances

Introduction

Lithium-ion batteries (LIBs) have been extensively used in portable electronic devices, and electric and electric hybrid vehicles. Considering the profound and lasting influence on human life, the safety and cycle life of LIBs are important, and largely depend on the electrode materials used.¹⁻⁴ Graphite is the most widely commercial anode material for LIBs, but suffers from poor rate capability and serious safety issues related to lithium dendritic growth especially at low temperature.⁴⁻¹⁵ Therefore, replacing graphite by other alternative anode materials is urgently required.

Among various candidates, spinel Li₄Ti₅O₁₂ is regarded as one of promising anode materials. It possesses many advantages over graphite. For example, Li₄Ti₅O₁₂ has a stable and flat operating voltage at 1.5 V, which can prevent the growth of lithium dendrites to achieve safe and reliable high-power LIBs.¹⁶⁻²² Meanwhile, it is a zero-train insertion material, which results in a brilliant cycling performance.²³⁻²⁶ However, its poor electronic conductivity, low Li-ion diffusion coefficient and especially the phenomenon of battery bloating seriously limit the applications at high rate and/or at high temperature.

More recently, LiCrTiO₄ has been comprehensively investigated due to its similar characteristics to Li₄Ti₅O₁₂.²⁷ LiCrTiO₄ also gives a similar potential at 1.5 V vs. Li/Li⁺ and a small volume change (less than 0.7%) during electrochemical cycling. Compared with Li₄Ti₅O₁₂, LiCrTiO₄ has a much higher electronic conductivity of 4 × 10⁻⁶ S cm⁻¹ and Li-ion diffusion coefficient of 10⁻⁹ cm² s⁻¹. We can image that LiCrTiO₄ should

be very promising as a high-rate and long-cycle anode for LIBs. To date, many efforts have been devoted to improving the electrochemical performance by using carbon coating, polymer incorporation and novel microstructure design.²⁷⁻³⁷ As we know, cationic doping is an effective method to enhance electrochemical performance of electrode materials in LIBs.³⁸⁻⁴⁰ For example, the Al substitution can significantly increase the reversible capacity and cycling stability of the LiNi_{1-*x-y*}Co_{*x*}Mn_{*y*}O₂ system due to the stable crystal structure after Al doping. Introduction of Al³⁺ has been proven to be effective to prevent the capacity fade.⁴¹⁻⁵¹

In order to achieve better rate and cycle performance of LiCrTiO₄, we employ Al doping in LiCrTiO₄ and try to

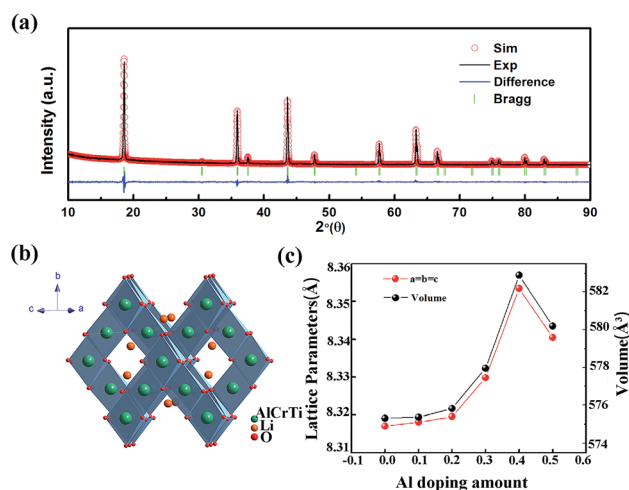


Fig. 1 (a) Rietveld refinement of XRD patterns of LiAl_{0.2}Cr_{0.8}TiO₄, (b) crystallographic arrangement of LiAl_{0.2}Cr_{0.8}TiO₄, (c) lattice parameters variation with Al doping amount.

School of Materials Science and Engineering, Huazhong University of Science and Technology, 1037 Luoyu Road, Wuhan, Hubei 430074, China. E-mail: jthan@hust.edu.cn; huangyh@hust.edu.cn



understand its role in electrochemical performance. Al-Doped LiCrTiO_4 samples have been successfully synthesized by a traditional solid-state reaction. The Al-doped LiCrTiO_4 exhibits an excellent rate performance and capacity retention. Comparing the electrochemical performances between Al-doped and pristine LiCrTiO_4 , we find that a small amount of Al doping can significantly improve rate capability and high-temperature performance of LiCrTiO_4 anode.

Experimental

In a typical solid-state reaction, stoichiometric starting materials Li_2CO_3 , TiO_2 , Al_2O_3 and Cr_2O_3 were thoroughly mixed,

ground in a mortar and pressed into pellets under a pressure of 20 MPa. Subsequently, the pellets were heated in a box furnace at 850 °C for 16 h in air and cooled down to room temperature naturally.

The phases of $\text{LiAl}_x\text{Cr}_{1-x}\text{TiO}_4$ were determined by X-ray diffraction (XRD, PANalytical B.V., Holland) with $\text{Cu K}\alpha$

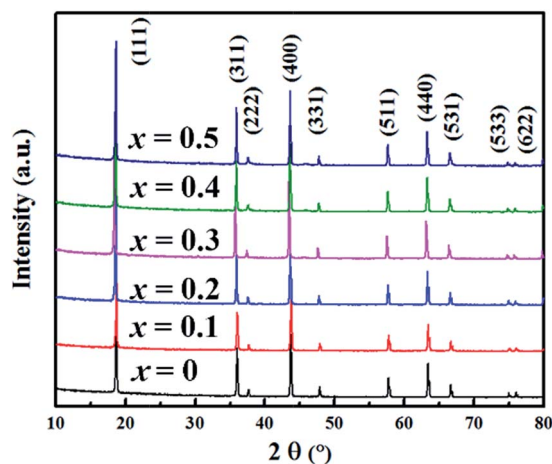


Fig. 2 XRD patterns for the prepared $\text{LiAl}_x\text{Cr}_{1-x}\text{TiO}_4$ ($0 \leq x \leq 0.5$) samples.

Table 1 Lattice parameters obtained by refinement of $\text{LiAl}_x\text{Cr}_{1-x}\text{TiO}_4$ ($0 \leq x \leq 0.5$)

Sample	$x = 0.1$	$x = 0.2$	$x = 0.3$	$x = 0.4$	$x = 0.5$
$a = b = c/\text{Å}$	8.3181(3)	8.3195(1)	8.3298(1)	8.3534(2)	8.3405(1)
$V/\text{Å}^3$	575.53(7)	575.82(3)	577.96(5)	582.89(5)	580.19(2)
R_p	11.34%	9.12%	10.26%	10.6%	12.47%
R_{wp}	8.34%	6.4%	7.36%	7.2%	8.54%

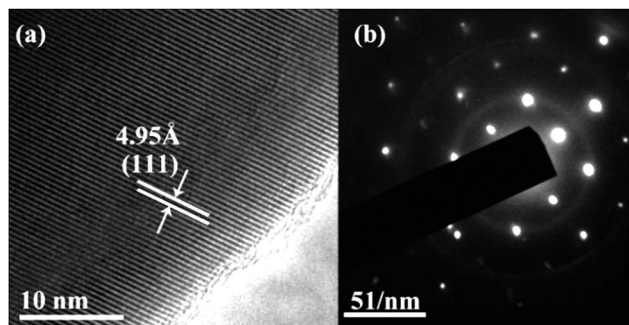


Fig. 3 (a) Transmission electron microscopic image of $\text{LiAl}_{0.1}\text{Cr}_{0.9}\text{TiO}_4$, (b) selected area electron diffraction (SAED) pattern of $\text{LiAl}_{0.1}\text{Cr}_{0.9}\text{TiO}_4$.

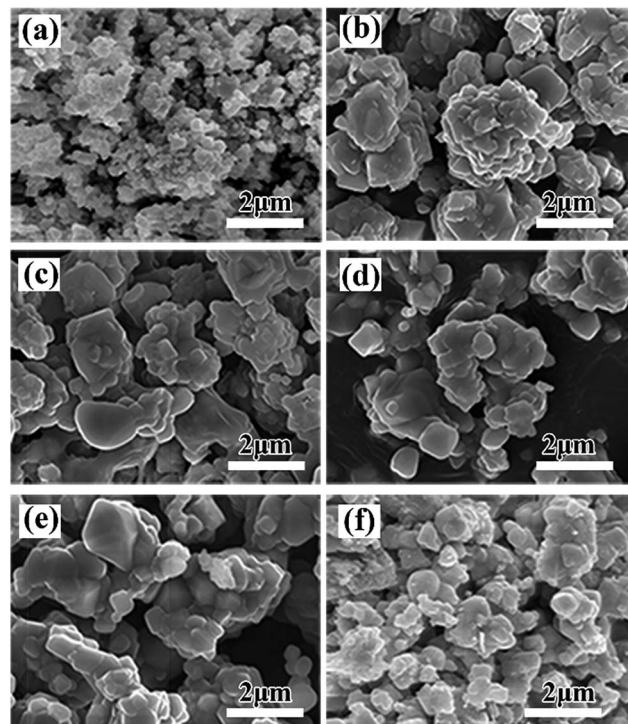


Fig. 4 SEM images of $\text{LiAl}_x\text{Cr}_{1-x}\text{TiO}_4$: (a) $x = 0.0$, (b) $x = 0.1$, (c) $x = 0.2$, (d) $x = 0.3$, (e) $x = 0.4$, (f) $x = 0.5$.

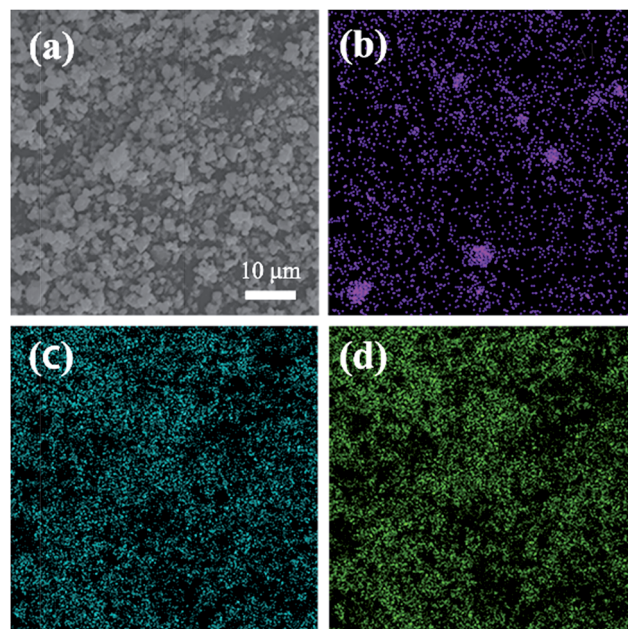
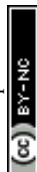


Fig. 5 Elemental mapping for the particles of the $\text{LiAl}_{0.2}\text{Cr}_{0.8}\text{TiO}_4$: (a) SEM image, (b) Al, (c) Cr, (d) Ti.



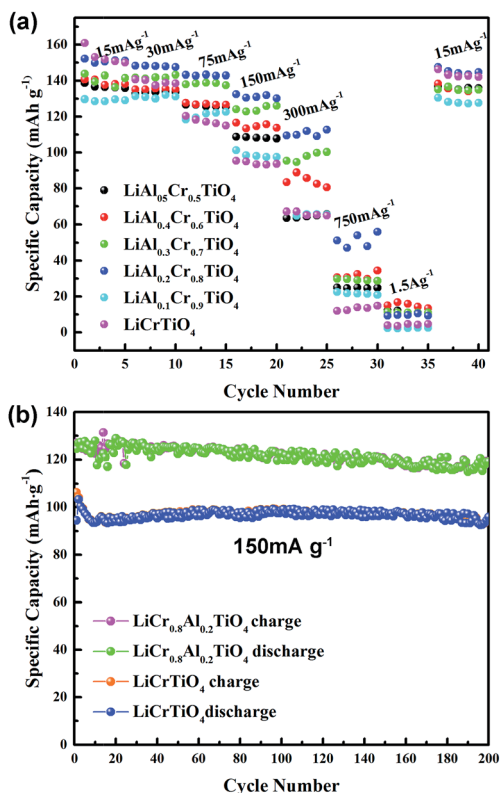


Fig. 6 Electrochemical properties of $\text{LiAl}_x\text{Cr}_{1-x}\text{TiO}_4$: (a) rate performance at different current rate from 0.1C to 10C, (b) specific capacity for 200 cycles at 150 mA h g^{-1} .

radiation of $\lambda = 1.5405 \text{ \AA}$. Rietveld refinement was carried out using the GSAS suite of programs with the EXPGUI interface. The morphology was observed by scanning electron microscopy (SEM, Nova nanoSEM 450) under 10 kV accelerating voltage. The high-resolution transmission electron microscopy (HR-TEM) images and selected area electron diffraction (SAED) patterns were recorded on a transmission electron microscope (JEM-2100).

Electrochemical performances were tested on CR2032 coin cells. The working electrodes were made from a slurry containing 80 wt% active material, 10 wt% C-black and 10 wt% polyvinylidene difluoride (PVDF) binder mixed in *N*-methyl pyrrolidinone (NMP). The slurry was pasted onto a copper foil. After being dried at $120 \text{ }^\circ\text{C}$ for 12 h in a vacuum oven, the foil was roll pressed and punched into round disks with a diameter of 8 mm. The loading of active material on each disk was $\sim 1.2 \text{ mg cm}^{-2}$. The counter electrode was lithium metal. The electrolyte was 1 mol L^{-1} LiPF_6 in a mixed solvent of ethylene carbonate and dimethyl carbonate (1 : 1 volume ratio). A thin sheet of microporous polyethylene (Celgard 2400) served as separator. The cells were assembled in an argon-filled glove box. Cyclic voltammetry (CV) was measured by an electrochemical workstation (PARSTAT MC, Princeton Applied Research, US) at a scan rate of 0.1 mV s^{-1} within a voltage range of 1.0–2.5 V. Electrochemical impedance spectroscopy (EIS) was also carried out on the PARSTAT MC with a potential amplitude of 5 mV in a frequency range of 10^5 to 10^{-1} Hz. Charge/discharge measurement was performed on a battery testing system (Land CT2001A, China) at $25 \text{ }^\circ\text{C}$ with various rates (0.1–5C).

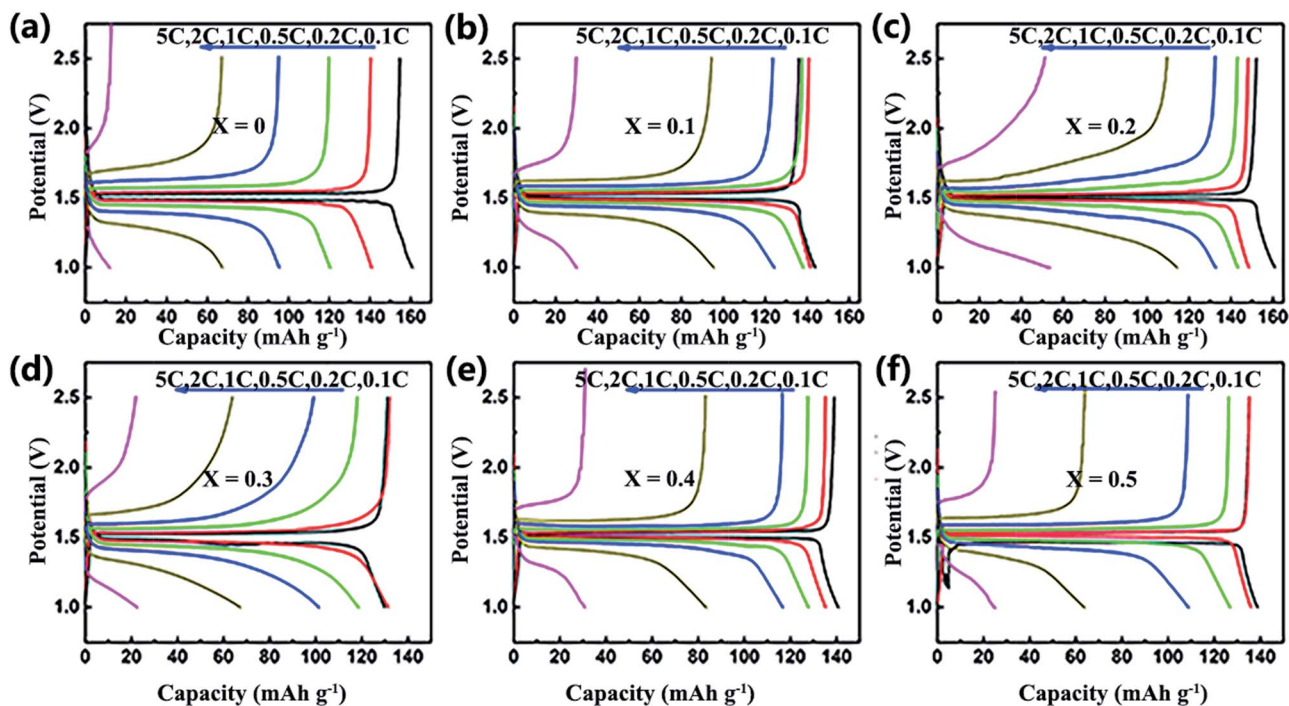


Fig. 7 Galvanostatic charge and discharge curves of first cycle measured at several rates in the range of 1–2.5 V for $\text{LiAl}_x\text{Cr}_{1-x}\text{TiO}_4$: (a) $x = 0$, (b) $x = 0.1$, (c) $x = 0.2$, (d) $x = 0.3$, (e) $x = 0.4$, (f) $x = 0.5$.



Results and discussion

Al-Doped LiCrTiO_4 can be readily synthesized *via* a conventional solid-state reaction. The XRD patterns of $\text{LiAl}_x\text{Cr}_{1-x}\text{TiO}_4$ ($x = 0-0.5$) are shown in Fig. 2. The diffraction peaks are indexed to the cubic spinel phase [space group 227, JCPDS no. 47-0139]. At a low-level Al doping, the difference in XRD patterns is not obvious. With increasing x , the diffractions slightly shift to high angles, demonstrating that Al substitution happens in the crystal lattice. Fig. 1a and c show the Rietveld refinement and the obtained lattice parameters, respectively. Table 1 lists the results of the refinements for $\text{LiAl}_x\text{Cr}_{1-x}\text{TiO}_4$ by assuming that Al ions are located at Ti sites. The best refinement model is based on $F\bar{3}m$ space group. With increasing x , lattice parameters a , b and c shrink while the cell volume becomes smaller. Since the ionic radius of Al^{3+} is smaller than that of Cr^{3+} , it is reasonable that the lattice parameters enlarged with increasing x . Corresponding to the Rietveld refinements in Table 1, Fig. 1b shows that Al^{3+} , Cr^{3+} and Ti^{4+} ions share the 16c position and Li^+ ions sit at 8b position, and the spinel structure keeps stable after the introduction of Al^{3+} ions. The reliability factor R_p of all the Rietveld refinements is below 10%, indicating the reliability of the refinement results. The lattice change of $\text{LiAl}_{0.1}\text{Cr}_{0.9}\text{TiO}_4$ is further identified by TEM and SAED, as shown in Fig. 3. The results agree well with the above description. The interplanar spacing of [111] is ~ 4.95 Å, much close to that of pristine LiCrTiO_4 .

Fig. 4 and 5 give SEM images of $\text{LiAl}_x\text{Cr}_{1-x}\text{TiO}_4$ samples. It is very clear that all the samples present irregular particles. Elemental mappings in Fig. 5 show that Al, Cr and Ti elements are uniformly distributed with less Al dispersion due to a small amount of dopant, which demonstrates that Al exists in the material proportionately.

Fig. 6a shows the discharge/charge capacities of the $\text{LiAl}_x\text{Cr}_{1-x}\text{TiO}_4$ electrodes at rates of 0.1–10C from 1.0 to 2.5 V. Apparently all the samples exhibited almost the same specific capacity close to the theory capacity at lower rate, as an increasing current, pure samples showed a rapid fading capacity of 95 mA h g^{-1} at 150 mA g^{-1} . The specific discharge capacities are 101, 132, 122, 113 and 109 mA h g^{-1} for $x = 0.1, 0.2, 0.3, 0.4$ and 0.5 , respectively. All samples deliver extremely low capacity at 1.5 A g^{-1} owing to the structure collapse. As shown in Fig. 6b, the $\text{LiAl}_{0.2}\text{Cr}_{0.8}\text{TiO}_4$ displays much better cyclability with a stable and broad charge/discharge plateau than LiCrTiO_4 , and its coulombic efficiency is nearly 100% at 1C during 200 cycles. It is obvious that the electrochemical performances of LiCrTiO_4 can be remarkably improved by Al doping.

Fig. 7 displays the initial charge/discharge curves of the $\text{LiAl}_x\text{Cr}_{1-x}\text{TiO}_4$ electrodes measured at different current densities within a voltage range of 1–2.5 V. Compared with pristine LiCrTiO_4 , the capacities of Al-doped LiCrTiO_4 are greatly enhanced, especially at high current densities. The improved rate capability can be ascribed to a kinetic effect that Al-doped LiCrTiO_4 has a high ionic conductivity as a host for Li-ion intercalation/extraction.

In order to investigate the comprehensive performances of Al-doped LiCrTiO_4 anodes, the cells were tested in a broad temperature range from 0 to 60°C at 1C. As shown in Fig. 8a, the gap between charge and discharge curves of LiCrTiO_4 becomes broader and the voltage plateau becomes shorter and shorter with decreasing temperature. Both the capacity and the discharge voltage plateau drop obviously as temperature decreases, which is ascribed to slow conductivity and high charge-transfer resistance of the electrode/electrolyte interface. Compared with LiCrTiO_4 , $\text{LiAl}_{0.2}\text{Cr}_{0.8}\text{TiO}_4$ delivers a better electrochemical performance at a broad temperature range (Fig. 8b). A possible mechanism might be that the Al doping improves the compatibility of the electrode materials with the organic electrolyte especially at high temperature and significantly reduces the asymmetric polarization in charge/discharge process at high rate.^{50–52} What's more, many practical applications require LIBs to be

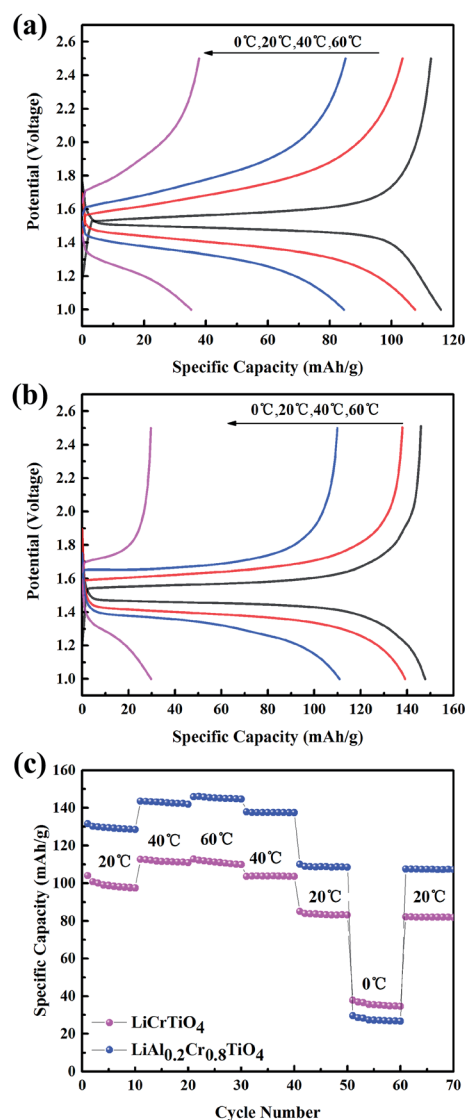


Fig. 8 (a) Galvanostatic charge and discharge curves of LiAlCrTiO_4 (b) $\text{LiAl}_{0.2}\text{Cr}_{0.8}\text{TiO}_4$, (c) the electrochemical performance of Al-doped and pristine samples at different temperature at 1C.



capable of operating within a larger temperature range even more than 60 °C.

Fig. 9 shows the CV curves of the pristine LiCrTiO₄ and the LiAl_{0.2}Cr_{0.8}TiO₄ at different scan rates from 0.1 to 1 mV s⁻¹ within 1.0–2.5 V. It can be seen obviously that there is one couple of reversible redox peaks, corresponding to the lithium insertion/extraction reactions. Fig. 9c displays the relationship between the cathodic peak current and the square root of the scan rate. It can be expressed by the classical Randles-Sevcik equation: $i_p = 2.69 \times 10^5 n^{3/2} A C_0 D^{1/2} \nu^{1/2}$, where i_p is the peak current, n is the number of electrons per molecule during the intercalation, A is the surface area of the anode, C_0 is the concentration of lithium ions [mol cm⁻³], D is the diffusion coefficient of lithium ions, and ν is the scan rate. Based on the above equation and the slopes of i_p vs. $\nu^{1/2}$ plots, the calculated Li-ion diffusion coefficients of LiCrTiO₄ and LiAl_{0.2}Cr_{0.8}TiO₄ are

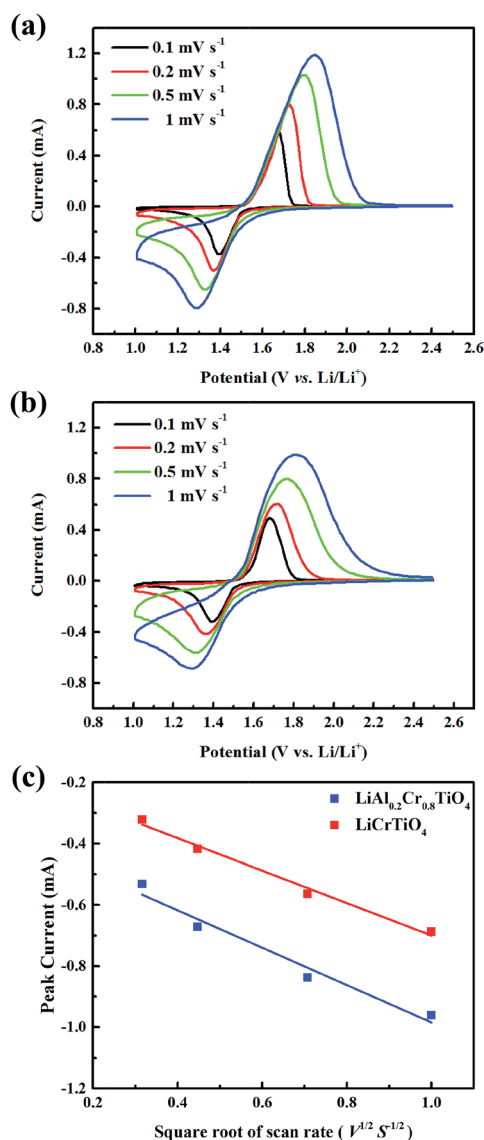


Fig. 9 CV curves at different rates for (a) LiAl_{0.2}Cr_{0.8}TiO₄ and (b) LiCrTiO₄; (c) relationship between the peak current (i_p) and square root of scan root ($\nu^{1/2}$).

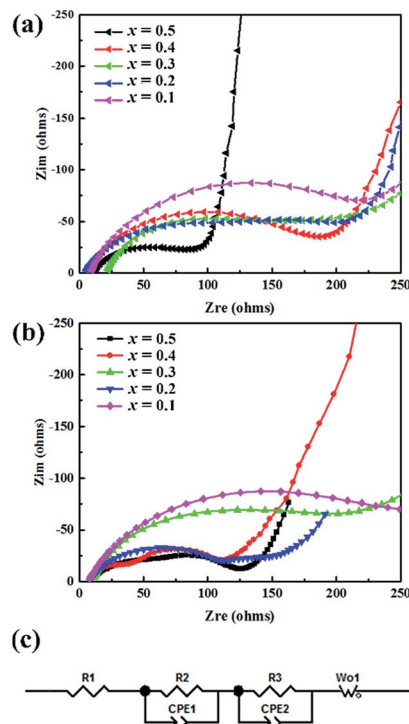


Fig. 10 AC impedance spectra of LiAl_xCr_{1-x}TiO₄/Li half-cell: (a) fresh cells, (b) after 100 cycles, (c) equivalent circuit of LiAl_{0.2}Cr_{0.8}TiO₄ electrode.

1.533×10^{-11} and 2.046×10^{-11} cm² s⁻¹, respectively. The results demonstrate that the Al-doped LiCrTiO₄ allows a higher Li-ion diffusion, which is in good agreement with the rate capabilities in Fig. 6.

We evaluated the internal resistance of lithium-half cells with EIS. In Fig. 10c. The resistance R_1 , R_2 and R_3 refer to the electrolyte resistance, charge transfer resistance and ionic migration through solid electrolyte interface (SEI), respectively. The CPE₁ and CPE₂ describe the capacitive behaviors between electrode and SEI, SEI and electrolyte, respectively. The W_{o1} represents the Warburg diffusion impedance. In Fig. 10a, the Nyquist plots reveal that the resistance varies with the Al doping level. The sloping line in low frequency corresponding to R_{ct} indicates that Li-ion diffusion resistance decreases due to gradual Al substitution, which suggests that the Al doping is beneficial to Li⁺-ion diffusion in the LiAl_xCr_{1-x}TiO₄ system. The Fig. 10b shows that the R_{ct} reduces gradually after 100 cycles, which also is in accord with the above results.

Conclusions

Al-Doped LiCrTiO₄ samples were synthesized by one-step solid-state reaction. The Rietveld refinement analysis shows that the Al-doped LiCrTiO₄ samples maintain the original spinel structure. The LiAl_{0.2}Cr_{0.8}TiO₄ exhibits a high capacity of 150 mA h g⁻¹ at a current density of 25 mA g⁻¹, which is close to its theoretical capacity of 157 mA h g⁻¹. It keeps a discharge capacity of 123 mA h g⁻¹ at 1C and 109 mA h g⁻¹ at 2C for 200 cycles. The Al-doped



LiCrTiO₄ electrodes show a stable cycle performance, especially at high temperature, with less asymmetric polarization. EIS results demonstrate that both electrode kinetics and ionic transport in LiCrTiO₄ are facilitated by Al doping. Consequently, the Al doping could be responsible for the high rate capacity and outstanding cycling stability. Our results show that LiCrTiO₄ is a promising anode material with high-rate and high-temperature performances for lithium-ion batteries.

Acknowledgements

This work is supported by the National High-Tech R&D Program of China (No. 2015AA034600, 2016YFB010030X and 2016YFB0700600), the China Postdoctoral Science Foundation (2016M590691). In addition, the authors thank Analytical and Testing Center of Huazhong University of Science and Technology for XRD, SEM and TEM measurement.

Notes and references

- J. M. Tarascon and M. Armand, *Nature*, 2001, **414**, 359–367.
- L. Zhao, Y.-S. Hu, H. Li, Z. Wang and L. Chen, *Adv. Mater.*, 2011, **23**, 1385–1388.
- P. Poizot, S. Laruelle, S. Grugeon, L. Dupont and J. M. Tarascon, *Nature*, 2000, **407**, 496–499.
- B. Luo and L. Zhi, *Energy Environ. Science*, 2015, **8**, 456–477.
- S. Han, D. Wu, S. Li, F. Zhang and X. Feng, *Adv. Mater.*, 2014, **26**, 849–864.
- D. Aurbach, B. Markovsky, I. Weissman, E. Levi and Y. Ein-Eli, *Electrochim. Acta*, 1999, **45**, 67–86.
- R. Yazami, *Electrochim. Acta*, 1999, **45**, 87–97.
- A. Funabiki, M. Inaba, Z. Ogumi, S. Yuasa, J. Otsuji and A. Tasaka, *J. Electrochem. Soc.*, 1998, **145**, 172–178.
- M. Winter, P. Novak and A. Monnier, *J. Electrochem. Soc.*, 1998, **145**, 428–436.
- M. Yoshio, H. Y. Wang, K. Fukuda, Y. Hara and Y. Adachi, *J. Electrochem. Soc.*, 2000, **147**, 1245–1250.
- D. Aurbach, E. Zinigrad, Y. Cohen and H. Teller, *Solid State Ionics*, 2002, **148**, 405–416.
- K. Takada, T. Inada, A. Kajiyama, H. Sasaki, S. Kondo, M. Watanabe, M. Murayama and R. Kanno, *Solid State Ionics*, 2003, **158**, 269–274.
- B. Fang, M.-S. Kim, J. H. Kim, S. Lim and J.-S. Yu, *J. Mater. Chem.*, 2010, **20**, 10253–10259.
- M.-S. Kim, B. Fang, J. H. Kim, D. Yang, Y. K. Kim, T.-S. Bae and J.-S. Yu, *J. Mater. Chem.*, 2011, **21**, 19362–19367.
- M.-S. Kim, D. Bhattacharjya, B. Fang, D.-S. Yang, T.-S. Bae and J.-S. Yu, *Langmuir*, 2013, **29**, 6754–6761.
- L. Zhao, Y. S. Hu, H. Li, Z. X. Wang and L. Q. Chen, *Adv. Mater.*, 2011, **23**, 1385–1388.
- L. Aldon, P. Kubiak, M. Womes, J. C. Jumas, J. Olivier-Fourcade, J. L. Tirado, J. I. Corredor and C. P. Vicente, *Chem. Mater.*, 2004, **16**, 5721–5725.
- A. S. Prakash, P. Manikandan, K. Ramesha, M. Sathiya, J. M. Tarascon and A. K. Shukla, *Chem. Mater.*, 2010, **22**, 2857–2863.
- E. M. Sorensen, S. J. Barry, H. K. Jung, J. R. Rondinelli, J. T. Vaughey and K. R. Poeppelmeier, *Chem. Mater.*, 2006, **18**, 482–489.
- H. G. Jung, S. T. Myung, C. S. Yoon, S. B. Son, K. H. Oh, K. Amine, B. Scrosati and Y. K. Sun, *Energy Environ. Science*, 2011, **4**, 1345–1351.
- K. Zaghbi, M. Simoneau, M. Armand and M. Gauthier, *J. Power Sources*, 1999, **81**, 300–305.
- K. S. Park, A. Benayad, D. J. Kang and S. G. Doo, *J. Am. Chem. Soc.*, 2008, **130**, 14930–14931.
- T.-F. Yi, S.-Y. Yang and Y. Xie, *J. Mater. Chem. A*, 2015, **3**, 5750–5777.
- H. H. Xu, X. L. Hu, W. Luo, Y. M. Sun, Z. Yang, C. C. Hu and Y. H. Huang, *ChemElectroChem*, 2014, **1**, 611–616.
- H. Xu, X. Hu, Y. Sun, W. Luo, C. Chen, Y. Liu and Y. Huang, *Nano Energy*, 2014, **10**, 163–171.
- T. Ohzuku, A. Ueda and N. Yamamoto, *J. Electrochem. Soc.*, 1995, **142**, 1431–1435.
- D. Liu, J. Han, M. Dontigny, P. Charest, A. Guerfi, K. Zaghbi and J. B. Goodenough, *J. Electrochem. Soc.*, 2010, **157**, A770.
- M. A. K. L. Dissanayake, R. P. Gunawardane, H. H. Sumathipala and A. R. West, *Solid State Ionics*, 1995, **76**, 215–220.
- M. A. Arillo, M. L. López, M. T. Fernández, M. L. Veiga and C. Pico, *J. Solid State Chem.*, 1996, **125**, 211–215.
- M. Nakayama, Y. Ishida, H. Ikuta and M. Wakihara, *Solid State Ionics*, 1999, **117**, 265–271.
- A. Kuhn, M. Martin and F. Garcia-Alvarado, *Z. Anorg. Allg. Chem.*, 2008, **634**, 880–886.
- C. V. Rao and B. Rambabu, *Solid State Ionics*, 2010, **181**, 839–843.
- V. Aravindan, W. Chuling and S. Madhavi, *J. Mater. Chem.*, 2012, **22**, 16026–16031.
- V. Aravindan, W. C. Ling and S. Madhavi, *ChemPhysChem*, 2012, **13**, 3263–3266.
- X. Y. Feng, C. Shen, N. Ding and C. H. Chen, *J. Mater. Chem.*, 2012, **22**, 20861–20865.
- L. Wang, Q. Z. Xiao, L. J. Wu, G. T. Lei and Z. H. Li, *Solid State Ionics*, 2013, **236**, 43–47.
- J. W. Yang, B. Yan, J. Ye, X. Li, Y. S. Liu and H. P. You, *Phys. Chem. Chem. Phys.*, 2014, **16**, 2882–2891.
- M. Abbate, S. M. Lala, L. A. Montoro and J. M. Rosolen, *Electrochem. Solid-State Lett.*, 2005, **8**, A288–A290.
- J. H. Lee, J. K. Hong, D. H. Jang, Y. K. Sun and S. M. Oh, *J. Power Sources*, 2000, **89**, 7–14.
- M. R. Yang and W. H. Ke, *J. Electrochem. Soc.*, 2008, **155**, A729–A732.
- P. F. Wang, P. Li, T. F. Yi, X. T. Lin, Y. R. Zhu, L. Y. Shao, M. Shui, N. B. Long and J. Shu, *J. Power Sources*, 2015, **293**, 33–41.
- M. M. Lao, P. Li, P. F. Wang, X. Zheng, W. J. Wu, M. Shui, X. T. Lin, N. B. Long and J. Shu, *Electrochim. Acta*, 2015, **176**, 694–704.
- J. Y. Lin, C. C. Hsu, H. P. Ho and S. H. Wu, *Electrochim. Acta*, 2013, **87**, 126–132.
- H. L. Zhao, Y. Li, Z. M. Zhu, J. Lin, Z. H. Tian and R. L. Wang, *Electrochim. Acta*, 2008, **53**, 7079–7083.



- 45 S. H. Park, K. S. Park, Y. K. Sun, K. S. Nahm, Y. S. Lee and M. Yoshio, *Electrochim. Acta*, 2001, **46**, 1215–1222.
- 46 A. R. Cho, J. N. Son, V. Aravindan, H. Kim, K. S. Kang, W. S. Yoon, W. S. Kim and Y. S. Lee, *J. Mater. Chem.*, 2012, **22**, 6556–6560.
- 47 S. T. Myung, N. Kumagai, S. Komaba and H. T. Chung, *Solid State Ionics*, 2001, **139**, 47–56.
- 48 A. B. Yuan, L. Tian, W. M. Xu and Y. Q. Wang, *J. Power Sources*, 2010, **195**, 5032–5038.
- 49 S. T. Myung, S. Komaba and N. Kumagai, *J. Electrochem. Soc.*, 2001, **148**, A482–A489.
- 50 T. Kakuda, K. Uematsu, K. Toda and M. Sato, *J. Power Sources*, 2007, **167**, 499–503.
- 51 L. F. Xiao, Y. Q. Zhao, Y. Y. Yang, Y. L. Cao, X. P. Ai and H. X. Yang, *Electrochim. Acta*, 2008, **54**, 545–550.
- 52 T. Yi, X. Hu and K. Gao, *J. Power Sources*, 2006, **162**, 636–643.

